

# Field-Induced Structural Transitions in Liquid Crystal Microemulsions

MinSu Kim, Ramesh Manda, DaYeon Lee, Jae-Won Lee, Asad Nauman, Hak-Rin Kim,\* and Seung Hee Lee\*

Liquid crystal (LC) droplets have fascinating properties, such as anisotropic properties, in response to external stimuli. As LC droplet size may determine the proper application of soft composites, various results from numerical simulations and experimental observations of LC droplets are reported. Here, detailed topological responses of individual bipolar droplets to electric fields, are shown. The integration of each response influences the entire electro-optic behavior. Monodispersed LC bipolar droplets are fabricated in a polyvinyl alcohol-dissolved aqueous solution via a membrane-emulsification method. The planar anchoring, provided by the polyvinyl alcohol surface, and surface elasticity, guide the entire LC director configuration, associated with topological defects, in the droplets. By simply blade-coating the solution, bipolar axes of the droplets can be randomly placed on a flat substrate. Two different subsequential stages are found when applying voltages: 1) director reorientation, which is threshold-less and 2) topological defect movement, which exhibits a threshold-like behavior. Various initial directions of the bipolar axes with respect to the field direction provide the transition voltage between these two stages. It is believed that this study can provide important clues to handle several fundamental issues in electro-optics of encapsulated LCs, such as the determination of response times, threshold, and operating voltages.

applications in sensors, photonic devices, and displays.<sup>[1–7]</sup> It is a well-known physical phenomenon that when a medium is surrounded by another immiscible medium, surface tension drives the spherical formation of dispersed phase to reduce the free energy of the system. The anisotropic nature of nematic LCs results in elasticity in such systems. The shape and size of LC droplets can be controlled from nano to microscale by adjusting the balance among the interfacial tension, surface anchoring, and elastic energy. This is achieved by appointing each medium in a system, for example, LC and another isotropic soft matter.<sup>[3,8–14]</sup> Regardless of the shape of LC droplets or emulsions, when the boundary condition of LC droplets or bulk LC alignment changes by external stimuli, these structural responses can be utilized as novel functional devices.<sup>[2,3,6,11,13,15]</sup> In such LC droplets, depending on the interfacial energy, surface anchoring (boundary condition), and elastic energy (bulk LC alignment), various configurations of LC

droplets can be formed, and topological defects inevitably occur in the system. For example, homeotropic anchoring results in the formation of a point defect at the center of a droplet, called a radial droplet (hedgehog configuration). Tangential anchoring leads to the formation of a pair of point defects (boojums) on the surface (bipolar configuration).<sup>[9,10,16,17]</sup> For example, polyvinyl alcohol (PVA) provides hydrophilic tangential anchoring to nematic LCs in emulsions. In a bipolar configuration with two boojums, where each boojum has a +1 topological charge, elastic deformations occur. Splay deformation occurs in the vicinity of boojums, and slight bend deformation occurs between the splay deformations. Thus, the bipolar configuration possesses a twofold cylindrical symmetry along the bipolar axis and an average nematic director through the two boojums. In contrast, the radial droplet forms a single hedgehog at the center of the droplets and possesses a spherical symmetry. Consequently, various types of LC configurations, such as twisted bipolar, toroidal, escaped radial, and twisted radial droplets, are generated because of the difference in the anchoring strength and elastic energy.<sup>[8,9,17]</sup> Alteration of external stimuli and surface anchoring allows these configurations to be interchangeable. The size of LC droplets also determines their configuration because the ratio of the elastic constant to the surface anchoring strength correlates with the droplet size, which

## 1. Introduction


The formation and structural transition of liquid crystal (LC) droplets is of great interest because of their feasibility for

M. Kim, D. Lee, S. H. Lee  
Department of Nano Convergence Engineering  
Jeonbuk National University  
Jeonju 54896, Republic of Korea  
E-mail: lsh1@jbnu.ac.kr

R. Manda, J.-W. Lee, A. Nauman, H.-R. Kim  
School of Electronic and Electrical Engineering  
Kyungpook National University  
Daegu 41566, Republic of Korea  
E-mail: rineey@knu.ac.kr

H.-R. Kim  
School of Electronics Engineering  
Kyungpook National University  
Daegu 41566, Republic of Korea

S. H. Lee  
Department of Polymer-Nano Science and Technology  
Jeonbuk National University  
Jeonju 54896, Republic of Korea

 The ORCID identification number(s) for the author(s) of this article can be found under <https://doi.org/10.1002/adom.202200563>.

DOI: 10.1002/adom.202200563

determines the critical radius responsible for different droplet configurations. Although direct observation of submicron-sized droplets under a polarized optical microscope is a difficult task, we can observe microscale LC droplets with a variety of droplet configurations.<sup>[9,10,16,17]</sup> The microscale results may help us indirectly understand nanoscale droplets.

Polymer-dispersed liquid crystals (PDLCs) are widely used in smart windows when the LC droplet size exceeds the visible wavelength. Microscale LC droplets can be fabricated by polymerization-induced phase separation, and upon the application of an electric field, the optical status switches between opaque and transparent modes. In this case, the difference in the refractive indices of the LC and polymer is a crucial factor to enhance the contrast ratio between the two switching modes, and the analysis of the field-induced LC alignment transition in PDLC droplets becomes important. For example, such PDLCs are in the normally scattering mode owing to the random distribution of LC droplets. This is bad from the viewpoint of energy saving because power is required to maintain the normally transparent mode as a normal glass window. By studying how LC formation and transition occur and applying the result to the system, we can develop a system that can maintain the transparent state without voltage application.

However, the droplet size of PDLC is random, and each drop size can result in different threshold voltages, thus leading to undetermined Fréedericksz transition in the system and hysteresis in the electro-optic responses.<sup>[18]</sup> In a monodispersed, uniformly aligned system, we can extend its application range owing to its controllable and predictable nature. For example, monodispersed objects can be spatially integrated in an array system for optical and photonic applications or for more precise control of the electro-optic modulation of the system.<sup>[19–22]</sup>

When the droplet size is below the visible wavelength and the refractive index of the polymer matrix is similar to that of the LC, the system is optically isotropic and transparent because scattering occurs weakly at the LC–polymer interface.<sup>[23,24]</sup> This normally transparent system switches its optical state between isotropic and anisotropic. In this switching mechanism, the polarization state of light is maintained when the light experiences an isotropic state upon geometrical deformation. Thus, the application can be extended to flexible–optical, photonic, and display devices with induced birefringence in the use of polarized light,<sup>[12,19,25–32]</sup> including the fabrication of elongated ellipsoidal droplets,<sup>[33,34]</sup> sliding surface droplets,<sup>[35]</sup> elongated chiral LC,<sup>[36]</sup> low-anchoring polymer surfaces,<sup>[37–39]</sup> and slippery interfaces.<sup>[40,41]</sup> However, the electro-optic behavior of such systems is not well understood and mostly appears as an electro-optic hysteresis. Thus, the analysis of the structural transition in LC droplets becomes important to determine whether the droplet size is larger or smaller than the visible wavelength. The observation of these microscale droplets via an optical microscope can provide a useful road map to predict the behavior of nematic director fields in micro or nanosized droplets, as well as the entire system.<sup>[2–6,10]</sup>

In this work, we focus on the field-induced reorientation mechanism of individual nematic bipolar droplets in terms of director reorientation and transition of bipolar axes (relocation of topological defects) under lateral electric fields. To facilitate the observations, we fabricate nematic LC microdroplets dispersed

in a PVA-dissolved aqueous solution, at which the monodispersity and in-plane distribution of bipolar axes are achieved by the Shirasu Porous Glass (SPG) membrane emulsifier. In this system, surfactants prevent the aggregation of droplets, and PVA provides tangential anchoring to the nematic LC, in which microemulsions based on stable bipolar droplets are produced. Lateral electric fields are applied to the bipolar droplets, where the bipolar axes are placed in the plane but randomly in the azimuthal direction. In this way, we explore a detailed reorientation and relaxation mechanism of individual droplets depending on their initial configuration and the direction of the applied electric fields. The structural transition occurs such that the director field continuously changes without a threshold before being fully aligned to the electric field direction, and topological defects relocate to minimize the free energy of the system. The electro-optic effect of each droplet is different owing to different directions of their defect-guided bipolar axes, even though their sizes are similar. We believe that this result can provide guidance for gaining insights into the structural design of droplets in such systems to achieve better electro-optic properties.

## 2. Theory

We consider a system that contains monodispersed bipolar droplets (radius  $R$ ), the easy axis  $\mathbf{n}_0$  of which is mainly aligned with the bipolar axes, which are randomly distributed in the azimuthal angle. The free energy of the system can be roughly described by the elastic, surface, and dielectric free energy densities:

$$f = \frac{WN}{4\pi R}(\mathbf{n}\cdot\mathbf{n}_0)^2 - \frac{KN}{2\pi R^2}(\mathbf{n}\cdot\mathbf{n}_0)^2 - \frac{\varepsilon_0\Delta\varepsilon N}{2}(\mathbf{n}\cdot\mathbf{E})^2 \quad (1)$$

where  $K$  is the Frank elastic constant with one elastic constant approximation and  $W$  is the anchoring coefficient, which represents the strength of the interaction between the LC and the surface for director rotation. The  $N$ ,  $R$ ,  $\varepsilon_0$ , and  $\Delta\varepsilon$  are the number density of the droplets, radius of the droplets, vacuum permittivity, and dielectric anisotropy, respectively. The first and second terms describe the elastic free energy density and the surface anchoring, respectively, in which the nematic director  $\mathbf{n}$  deviates from  $\mathbf{n}_0$ , and the third term describes the dielectric free energy density, where  $\mathbf{n}$  interacts with  $\mathbf{E}$ . The required electric field strength can then be described as

$$E \approx \sqrt{\frac{1}{\varepsilon_0\Delta\varepsilon R} \left( \frac{W}{2\pi} - \frac{K}{\pi R} \right)} \quad (2)$$

where  $R \gg K/W$ ; we can neglect the free energy term of the anchoring strength at the droplet surface because of the strong anchoring that causes elastic deformation at the surface. Where  $R \ll K/W$ , however, the anchoring strength is important for the threshold electric field.

The torque exerted on the local director in the droplet can also be evaluated. Under an electric field, the dielectric energy can be described as

$$\frac{\mathcal{E}(E)}{\varepsilon_0} = \varepsilon_{\perp} \sin^2 \phi E^2 + \varepsilon_{\parallel} \cos^2 \phi E^2 \quad (3)$$

then the torque is

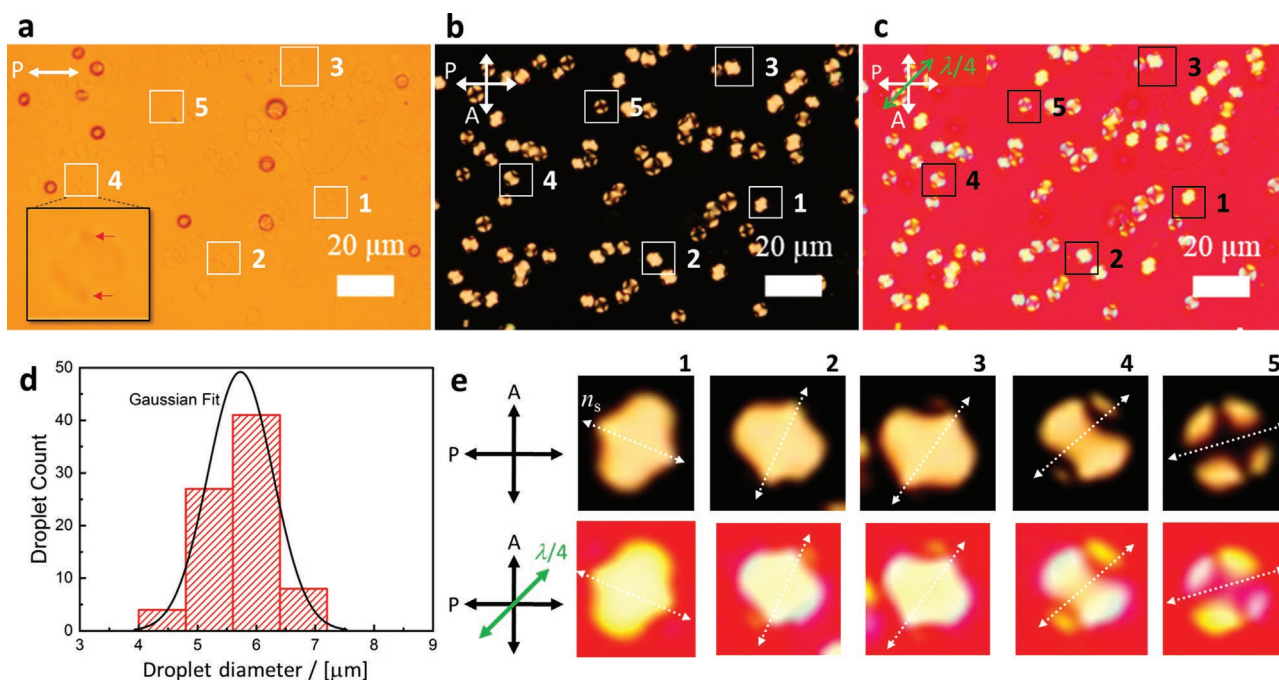


**Figure 1.** POM images of the microemulsions observed with a) a single polarizer, b) crossed polarizers, and c) a quarter-wave plate placed by 45° in between crossed polarizers. d) Size distribution of LC droplets. e) White-dotted arrows indicate the nematic director  $n_d$  of each bipolar droplet on average. P and A indicate polarizers.

$$|T| = \frac{\partial \mathcal{E}(E)}{\partial \phi} = \Delta \epsilon \epsilon_0 \sin 2\phi E^2 \quad (4)$$

where  $\phi$  is the angle between  $\mathbf{n}$  and  $\mathbf{E}$ . The torque is strongest when  $\phi = \pi/4$  and the weakest when  $\phi = 0$  or  $\pi/2$ .

### 3. Results and Discussion

Monodispersed spherical LC droplets on the microscale were obtained by using an SPG porous membrane with a pore size of 1.5  $\mu\text{m}$  at 50 °C, as shown in **Figure 1**. The obtained microemulsions were stable with no coalescence, as shown in **Figure 1a–c**. The PVA shell provides planar anchoring of LC emulsions and forms bipolar droplets with the nematic director  $n_d$  aligned between two-point defects along the bipolar axis on average. **Figure 1a** shows an optical microscope image under a single polarizer that exhibits the spatial position of point defects, as indicated by the red arrows in the inset, by slight light scattering due to abrupt changes in the refractive index near the point defects. The polarizing optical microscope (POM) images with crossed polarizers in **Figure 1b** show typical birefringence patterns of bipolar droplets. In **Figure 1c**, the POM images are taken with crossed polarizers and a quarter-wave plate (QWP) inserted at 45° to the polarizers. The QWP contributes to bluish and yellowish colors that provide information on the anisotropic alignment direction of the nematic directors in droplets. The optical textural evolution of the rotated sample is shown in **Figure S2**, Supporting Information. The average size is measured as  $5.7 \pm 0.5 \mu\text{m}$  in **Figure 1d**. The full width at half maximum of the Gaussian fit curve is 1.3  $\mu\text{m}$ . To measure the PVA shell thickness, we fabricated another cell in which

excess PVA in the continuous aqueous phase was additionally polymerized after blade coating. The PVA shell, surrounded by an excess polymer matrix, is thus sufficiently strong to stand after the removal of LCs by n-hexane solvent and remains observable. The droplet size in **Figure S3**, Supporting Information is different from that in our work, and the aspect ratio of the shells can be higher (owing to the removal of LCs). However, a field emission scanning microscope (FESEM) image of the polymer matrix (**Figure S3**, Supporting Information) shows a PVA shell thickness of less than 100 nm. From the FESEM observation, we also found that the LC droplets were not fully spherical but spheroidal. After blade coating, the droplets become oblate, that is, the shape anisotropy makes the droplets bipolar with a high possibility. Among the droplets in the image, we focused on five bipolar droplets, as indicated by the white squares in **Figure 1a–c**. The detailed director configuration of the bipolar droplets is shown in **Figure S4**, Supporting Information. The POM images of each droplet in **Figure 1e** show the possible variation in the azimuthal direction of the droplets.

We investigated the electric-field-dependent structural transition of bipolar droplets under lateral electric fields, as shown in **Figure 2**. We focused on three droplets with spatial positions between the electrodes to observe the field-induced reorientations. These droplets are marked with dotted white squares. The  $n_d$  completely differed in each droplet to study their responses to the electric fields. A POM image with a single polarizer shows the LC alignment and boojums in a droplet in the top-first column. Without a field,  $n_d$  has no preferential azimuthal direction. Under an applied electric field, the LCs are aligned along the field direction, thereby resulting in a lateral distortion in the director profile.

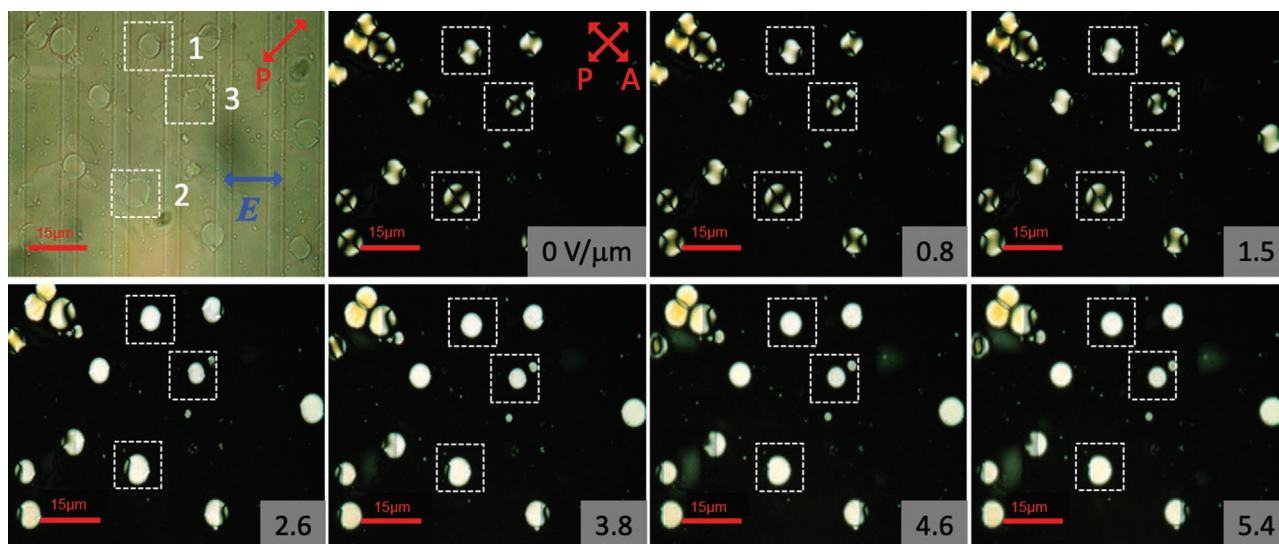


**Figure 2.** Topological transitions of bipolar droplets under lateral electric fields. The white-dotted squares indicate observed droplets. The red and blue arrows indicate polarizers and an electric field, respectively.

We closely observed individual droplets to investigate the topological transitions, as shown in **Figure 3**. The three different orientations of the bipolar droplets possess different azimuthal angles  $\delta$  (the angle between  $\mathbf{n}_d$  and  $\mathbf{E}$ ) at  $44^\circ$ ,  $62^\circ$ , and  $2^\circ$ , as shown in Figure 3a–c, respectively. As the electric

field is increased, the LC directors reorient along the electric field direction such that the free energy of the system is minimized, in which the elastic, interfacial, and electric energies are involved. As shown in Figure 3a–c,  $\delta$  changes to near  $0^\circ$  at the final, regardless of the initial  $\mathbf{n}_d$  as the initial and final

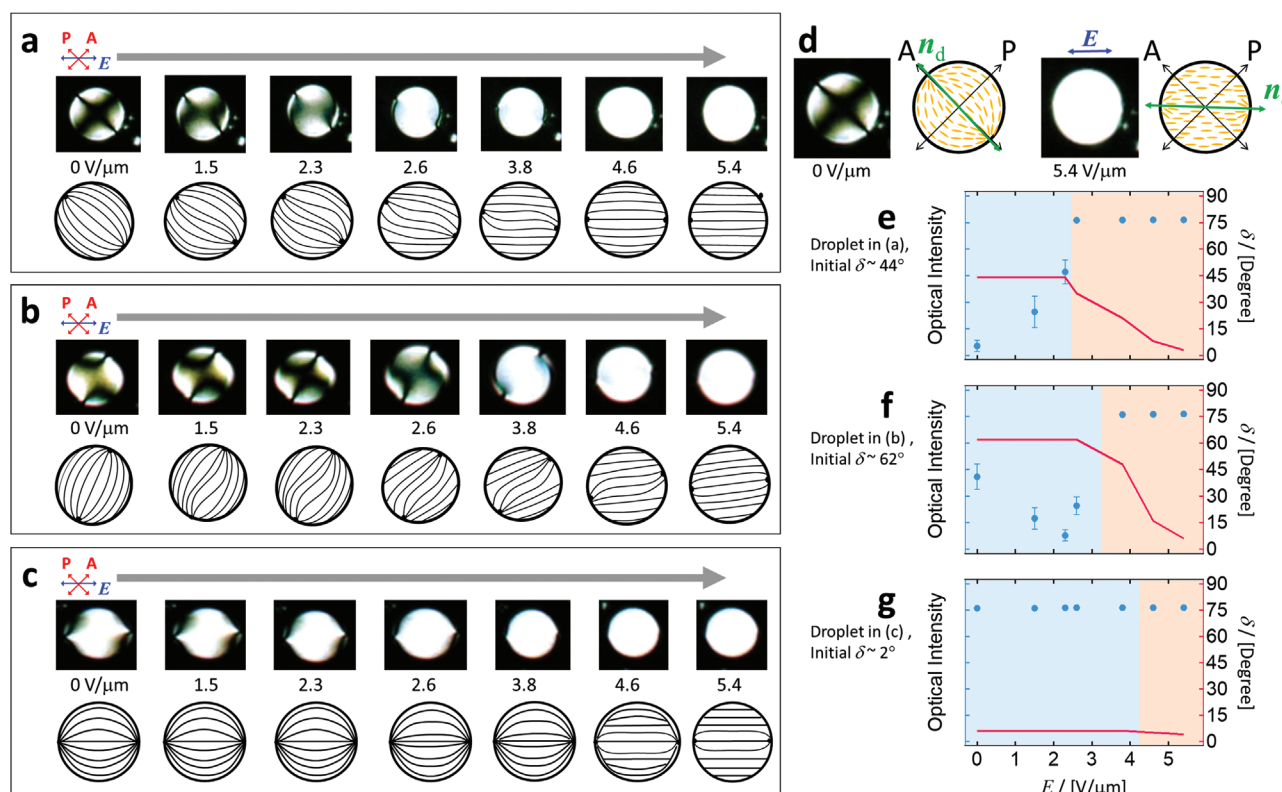


**Figure 3.** Structural evolution of bipolar droplets with various  $\mathbf{n}_d$  with respect to electric field  $E$  where the angle  $\delta$  between  $\mathbf{n}_d$  and  $\mathbf{E}$  is  $\approx$  a)  $44^\circ$ , b)  $62^\circ$ , and c)  $2^\circ$ . d) Director fields corresponding to the POM images of the droplet in (a). e–g) Optical intensity and electric field-dependent  $\delta$  of the droplets in (a–c).

droplet configurations shown in Figure 3d. Here, the difference between each of the three cases is how the LC local reorientation occurs before  $\delta$  begins to change. The POM images and the LC director field obtained based on the optical polarization analysis show that LC reorientation first arises in the center regions. Next, as the field strength is increased, the entire droplet, including the area near the boojums, turns into a nearly uniform alignment, showing a bright state under the crossed polarizers.

In Figure 3e–g, we plot the optical intensity measured in the area over the distance half of the diameter from the center of the droplet and  $\delta$  with respect to  $E$  for the three different cases of Figure 3a–c. When the initial  $\delta = 44^\circ$ , the optical intensity gradually and continuously increases and reaches the saturation value (at  $\approx 2.5 \text{ V } \mu\text{m}^{-1}$ ) in Figure 3e. Near this electric field strength,  $\delta$  begins to decrease and almost reaches  $0^\circ$  (at  $5.4 \text{ V } \mu\text{m}^{-1}$ ). When the electric potential is increased, once the LC reorientation reaches the point where the molecules are almost aligned along the electric field direction, the LC directors around the boojums begin to reorient along the electric field direction. In this stage, the LC directors around the boojums try to maintain their orientation perpendicular to the defect point to maintain the +1 charge and the elastic free energy minimum. This gives rise to the two boojums moving to the edge of the droplets along the field direction so that  $\delta$  changes to near zero. As the electric field strength is decreased, the LC directors relax back to the original configuration, as shown in Figure S5, Supporting Information.

This mechanism works similarly in other cases where the initial  $\delta$  is  $62^\circ$  and  $2^\circ$ , as shown in Figure 3f,g. However, in Figure 3f, where  $\delta = 62^\circ$ , the optical intensity first decreases and then increases as the LC molecules follow the electric field direction around the center region of the droplets. Here, the local LC reorientation stage covers a larger voltage range (bluish in Figure 3e,f), and the change in  $\delta$  covers a smaller voltage range (reddish in Figure 3e,f) than when the initial  $\delta = 44^\circ$ , as shown in Figure 3e,f. This is because the LC molecules have a greater degree of rotation until they are almost aligned to the electric field. When the initial  $\delta = 2^\circ$ , the LC molecules are already aligned along the electric field direction so that there is a minor change in both the optical intensity and  $\delta$ , as shown in Figure 3g. To understand the results further, we discuss the local LC directors by considering the torque exerted on the LC local director. Based on Equation (4), the dielectric torque is the maximum where  $\phi = \pi/4$ . The torque is the strongest when  $\delta = 44^\circ$ , intermediate when  $62^\circ$ , and the weakest when  $2^\circ$  among the three cases, as some estimated values are plotted in Figure S6, Supporting Information. Considering  $\delta = 44^\circ$ ,  $62^\circ$ , and  $2^\circ$ , the main orientations of the local LC directors also follow  $\delta$  because the two boojums in the droplets are a hedgehog configuration and the directors are almost aligned along the direction between boojums.

From Figure 3e–g, the measured result shows that the local LC reorientation behavior does not appear to be a specific threshold electric field. The threshold electric field can be estimated as a function of  $W$  (assuming  $R = 3 \text{ } \mu\text{m}$ ) and  $R$  (assuming  $W = 10^{-4} \text{ N m}^{-1}$ ) from Equation (2), assuming  $K = 10 \text{ pN}$  and  $\Delta\epsilon = 30$ , as shown in Figure 4a. The plot shows that, when  $R > 0.2 \text{ } \mu\text{m}$  and  $W = 10^{-4} \text{ N m}^{-1}$ , as the anchoring

coefficient of the PVA surface measured in a previous study,<sup>[42]</sup>  $E_{\text{th}}$  does not exceed  $0.3 \text{ V } \mu\text{m}^{-1}$ , being consistent with the behavior of non-specific threshold electric field. When  $R < 0.2 \text{ } \mu\text{m}$ , the initial LC droplet configuration changes because the critical length  $K/W > 2R$ . Similarly, when  $R = 3 \text{ } \mu\text{m}$  and  $10^{-5} < W < 10^{-3} \text{ N m}^{-1}$ ,  $E_{\text{th}}$  also does not exceed  $0.5 \text{ V } \mu\text{m}^{-1}$ .

Further, the time-dependent response of the LC droplets with variation in the initial  $\delta$  should be explored. We verify that the LC droplets return to the original configuration after the field-induced structural transitions upon removal of the electric field. We applied  $E = 5.4 \text{ V } \mu\text{m}^{-1}$  to the LC droplets with the initial  $\delta = 50^\circ$ ,  $23^\circ$ , and  $12^\circ$ , as shown in Figure 4b–d, respectively. Although the initial  $\delta$  in this observation is different from that in the electric-field-dependent transmittance measurement result, we observe a similar tendency. The measured time-dependent transmittance curves show  $\tau_{\text{on}} (\tau_{\text{off}}) = 0.8 (1.0)$  at the initial  $\delta = 50^\circ$  (Figure 4b),  $\tau_{\text{on}} (\tau_{\text{off}}) = 0.7 (0.9)$  at the initial  $\delta = 23^\circ$  (Figure 4c), and  $\tau_{\text{on}} (\tau_{\text{off}}) = 0.7 (0.8)$  at the initial  $\delta = 12^\circ$  (Figure 4d), as summarized in Table 1. Basically,  $\tau_{\text{on}}$  is shorter than  $\tau_{\text{off}}$  because, when switching off, the relaxation is only governed by the elastic energy and the anchoring strength, whereas the electric energy is additionally involved in shortening the response time when switching on. As the initial  $\delta$  decreases, the response times become quicker because the degree of the reorientation for returning back to the original configuration takes a shorter time. When an electric field ( $5.4 \text{ V } \mu\text{m}^{-1}$ ) is applied, as shown in each POM image of the second column in Figure 4b–d, the LC molecules reorient entirely and simultaneously in the droplet because simultaneous elastic deformation occurs over the entire area. This causes different LC responses when the field strength is swept. Upon removal of the electric field, relaxation first occurs in the area where the local LC directors are strongly deformed, and then relaxation occurs sequentially in the rest of the area. When the voltage is on, the optical intensity (local reorientation) first increases, and then  $\delta$  changes. Similarly, when the voltage is off, the optical intensity (local reorientation) first decreases, and then  $\delta$  changes, as shown in the POM images of each droplet in Figure 4b–d.

We also compared our result with another previous report on a flat PVA surface.<sup>[43]</sup> The switching-off time therein is  $\approx 30 \text{ min}$  to rotate an angle of  $\pi/4$  after the removal of  $5 \text{ V } \mu\text{m}^{-1}$ , which is significantly slower than the switching-off time of the LC emulsion in our work. We believe this is because of the elastic confinement effect and contribution of polar anchoring in the droplet; the reason for the polar anchoring involvement can be understood by the curved surface of the droplets. The initial LC directors are not aligned uniformly in a single direction before coupling  $\mathbf{n}(\mathbf{r}) \times \mathbf{E}$  occurs on the local points of the spherical soft surface of the droplets. Each single molecule experiences a different torque (but probably in a continuous variation) in the electric field direction when considering it in 3D. In contrast, the movement of topological defects and changes in  $\delta$  can be explained by the addition of energetic competition between the topological defects and elastic deformation that degenerates the defects under electric fields. The boojums can be anchored by the surface and elastic energies, where the system can be considered with the elastic, surface anchoring (including the geometric effect of PVA shells), dielectric, and defect terms.

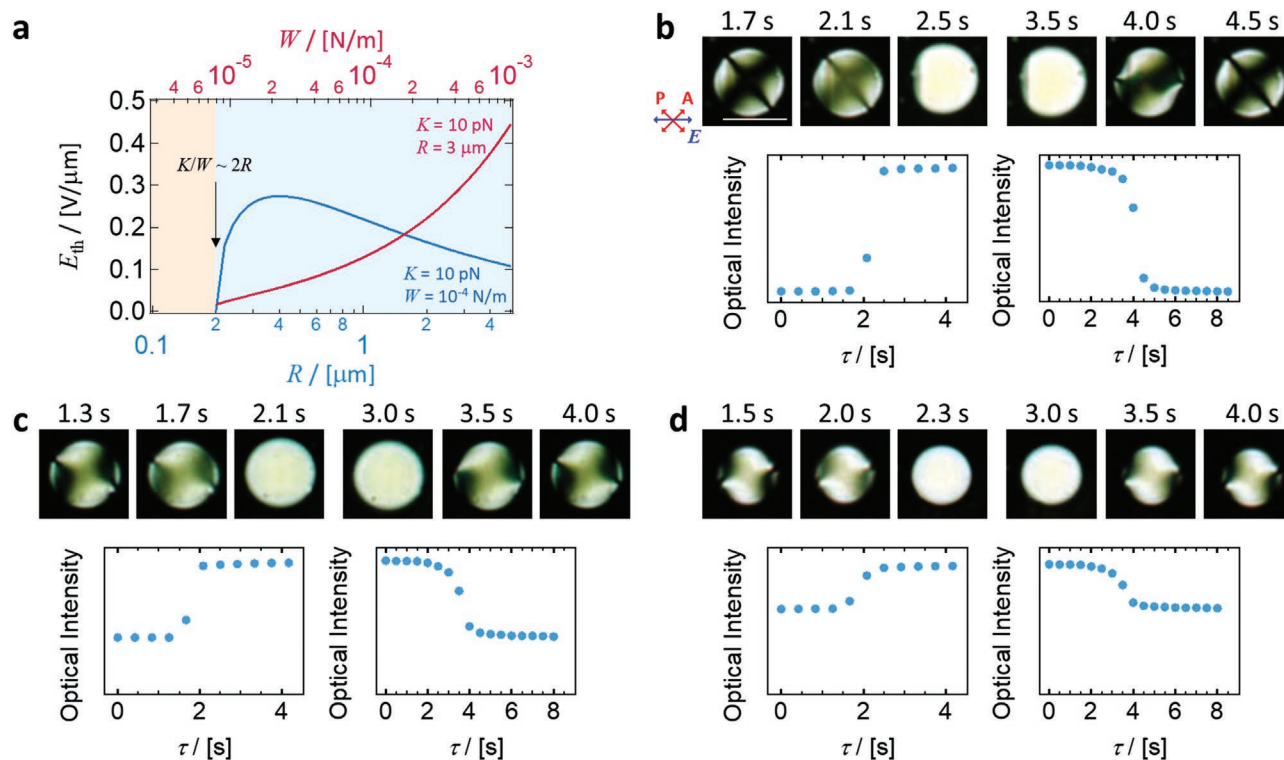


**Figure 4.** a) Estimation of the threshold electric field  $E_{th}$  as a function of the anchoring coefficient  $W$  and radius of cavities  $R$ . The droplet configuration and response times  $\tau$  of the LC droplets upon the application of the electric field  $E = 5.4 \text{ V } \mu\text{m}^{-1}$  when the initial  $\delta =$  b)  $50^\circ$ , c)  $23^\circ$ , and d)  $12^\circ$ . The scale bar is  $10 \mu\text{m}$ .

Based on the results of our observations and measurements, we can deduce that in a system with many bipolar droplets with random orientations, the electro-optic properties, including threshold, operation voltages, and response times, can be the integration of individual electro-optic responses of each bipolar droplet. Upon collection of the electro-optic responses of all droplets, the field-strength-dependent transmittance curve becomes rather intricate and does not exhibit a clear single behavior. We strongly believe that such complex electro-optic behaviors of the droplets should be considered in the entire system by integrating the behavior of each droplet.

#### 4. Conclusion

In this work, we study the reorientation and configuration transition mechanisms of nematic bipolar droplets under lateral electric fields. Monodispersed LC microemulsions were well produced in a PVA-dissolved aqueous solution, and bipolar LC droplets were softly blade-coated on a substrate to observe their behavior when their bipolar axes were parallel to the plane of the substrate. By applying lateral electric fields, these bipolar droplets could be continuously reoriented. At the point where the electric potential exceeded the surface anchoring strength to align the LC molecules, topological defects moved to both ends of the droplets along the electric field direction to minimize the defect energy with respect to the aligned director field. As the initial direction of the defect-guided bipolar axis with respect

to the electric field direction differed, the transition-electric field strength between the continuous reorientation of the LC molecules and the topological defect movements changed. A larger deviation angle between the bipolar axis and the electric field direction resulted in a higher operation electric field. We also verified the dynamics of the LC droplets upon the application and removal of electric fields close to the operating electric field strength. The results clearly show that the bipolar droplets are fully reversible. Unlike the field-strength-dependent transmittance behavior, the time-dependent response shows different LC reorientation behaviors. When switching on, simultaneous LC reorientation occurs over the entire area, but when switching off, the deformed LC directors relax back locally owing to the lack of electric fields. We believe that these findings contribute to solving the long-standing, fundamental issue of hysteresis in electro-optic responses in systems with integrated droplets, which possess a wide range of potential applications in flexible and transparent displays and photonic devices.

**Table 1.** Response times of LC droplets under  $E = 5.4 \text{ V } \mu\text{m}^{-1}$ .

Initial $\delta$ [ $^\circ$ ]	$\tau_{on}$ [s]	$\tau_{off}$ [s]
50	0.8	1.0
23	0.7	0.9
12	0.7	0.8

## 5. Experimental Section

**Materials:** An aqueous medium that consists of polyvinyl alcohol (5 wt%, PVA, density = 1.19–1.31 g cm<sup>-2</sup>, melting point = 200 °C, and refractive index = 1.477 at 632 nm) and deionized water (95 wt%) was prepared. Nematic LC microemulsions were fabricated by mixing nematic LC (50 wt%, nematic to isotropic transition  $T_{NI} = 68$  °C,  $n_e = 1.6442$ ,  $n_o = 1.4950$ ,  $\Delta n = 0.1492$  at 589 nm,  $\Delta\epsilon = 30.1$  at 20 °C and 1 kHz, rotational viscosity  $\gamma_1 = 279$  mPa·s, MAT-07-1251, Merck Advanced Technology, Korea) with the prepared aqueous medium via a porous membrane emulsification technique (Shirasu porous glass [SPG] emulsifier, IMK-40, MCTech. Co.), as shown in Figure S1a, Supporting Information.

**Emulsification:** In the emulsifying process, the dispersed phase was pushed under pressure, applied by N<sub>2</sub> gas, into a continuous phase through a hydrophilic porous membrane flow at a constant flow rate. The structure of the membrane used in this study is shown in Figure S1b, Supporting Information. LC droplets formed on the other side of the membrane, depending on the continuous phase flow velocity and the membrane pore size. The shear force of the continuous phase partially dragged dispersed LC into water, which determined the droplet size. By controlling the emulsification parameters, such as the flow rate of the continuous phase, rotational speed of the cylinder, and pressure applied on the dispersed phase, monodispersed spherical LC microemulsions were obtained through the porous membrane (Figure S1, Supporting Information).<sup>[15,44]</sup> The membrane (pore size, 1.5 μm) was used at a stirring speed (200 rpm) and a sample temperature (50 °C), where N<sub>2</sub> gas was pressured (45 kPa). The size of the produced emulsion was measured (5.7 ± 0.5 μm). These parameters were optimized by fabricating several test samples according to previously reported methods.<sup>[15,45]</sup>

**Cell Fabrication and Characterization:** Several techniques were used to study the field-induced topological transition of the LC droplets, to characterize the obtained microemulsions. The emulsion solution was brush-coated onto a glass substrate before the optical textures of the LC droplets were observed. The director profile of the LC droplets was analyzed by observing the relevant optical textures using a polarizing optical microscope (POM, Eclipse E600 POL, Nikon) with a CCD camera (DXM 1200, Nikon). The lateral electric field was formed by interdigitated patterned indium–tin oxide electrodes with the electrode width  $w = 4$  μm and the distance between the electrodes  $l = 11$  μm. A sinusoidal wave with a frequency of 1 kHz was applied by using a function generator (AFG3101C, Tektronix) and a voltage amplifier (A400, FLC Electronics). The electro-optic effect of each droplet was measured via post-image processing using open-source software (ImageJ, NIH). The PVA shells with a polymer matrix were observed by FESEM (SUPRA40VP, Carl Zeiss) installed in the Center for University-wide Research Facilities (CURF) at the Jeonbuk National University.

## Supporting Information

Supporting Information is available from the Wiley Online Library or from the author.

## Acknowledgements

This work was supported by the Regional Leading Research Center Program through the National Research Foundation (NRF), Korea, funded by the Ministry of Science and ICT, Korea [2019R1A5A8080326]; the Basic Science Research Program through the National Research Foundation (NRF), Korea, funded by the Ministry of Education [2021R111A1A01060001]; and by the ITECH R&D Program of MOTIE/KEIT (Ministry of Trade, Industry & Energy/Korea Evaluation Institute of Industrial Technology) [20016808]. This work was also supported by the National Research Foundation of Korea (NRF) grant No. 2019R1A2C1005531. The authors

would like to thank Prof. Francesca Serra and Prof. Shin-Woong Kang for their valuable discussions on this work.

## Conflict of Interest

The authors declare no conflict of interest.

## Author Contributions

M.S.K. and R.M. contributed equally to this work. *Analyzed the results and wrote and revised the manuscript:* M.S.K. *Prepared the samples and performed experiments:* R.M. *Summarized the results:* D.Y.L., J.W.L., and A.N. *Provided comments on the edition:* H.R.K. *Project initiation and conception:* S.H.L.

## Data Availability Statement

The data that support the findings of this study are available from the corresponding author upon reasonable request.

## Keywords

bipolar droplets, electro-optics, encapsulation, liquid crystals, microemulsions

Received: March 10, 2022

Revised: May 27, 2022

Published online: July 13, 2022

- [1] E. Brasselet, N. Murazawa, H. Misawa, S. Juodkakis, *Phys. Rev. Lett.* **2009**, *103*, 103903.
- [2] S. Sivakumar, K. L. Wark, J. K. Gupta, N. L. Abbott, F. Caruso, *Adv. Funct. Mater.* **2009**, *19*, 2260.
- [3] J. K. Gupta, S. Sivakumar, F. Caruso, N. L. Abbott, *Angew. Chem., Int. Ed.* **2009**, *48*, 1652.
- [4] I. H. Lin, D. S. Miller, P. J. Bertics, C. J. Murphy, J. J. De Pablo, N. L. Abbott, *Science* **2011**, *332*, 1297.
- [5] D. S. Miller, N. L. Abbott, *Soft Matter* **2012**, *9*, 374.
- [6] D. S. Miller, X. Wang, N. L. Abbott, *Chem. Mater.* **2013**, *26*, 496.
- [7] J. Yoshioka, F. Araoka, *Nat. Commun.* **2018**, *9*, 432.
- [8] P. S. Drzaic, *Liquid Crystal Dispersions*, World Scientific Publishing Co. Pte. Ltd., Singapore, **1995**.
- [9] P. S. Drzaic, A. Muller, *Liq. Cryst.* **2008**, *5*, 1467.
- [10] O. D. Lavrentovich, *Liq. Cryst.* **2010**, *24*, 117.
- [11] S. Bronnikov, S. Kostromin, V. Zuev, *J. Macromol. Sci., Part B: Phys.* **2013**, *52*, 1718.
- [12] R. Manda, J. H. Yoon, S. Pagidi, S. S. Bhattacharyya, D. T. T. Tran, Y. J. Lim, J.-M. Myoung, S. H. Lee, *Opt. Express* **2019**, *27*, 34876.
- [13] Z. Sumer, F. A. Fernandez, A. Striolo, *Nanoscale* **2020**, *12*, 20211.
- [14] K. Peddireddy, S. Čopar, K. V. Le, I. Mušević, C. Bahr, V. S. R. Jampani, *Proc. Natl. Acad. Sci. USA* **2021**, *118*, e2011174118.
- [15] D. C. Bao, H. A. Zhang, X. D. Liu, Y. J. Zhao, X. J. Ma, Q. Yuan, *J. Dispersion Sci. Technol.* **2007**, *28*, 485.
- [16] P. Drzaic, *Mol. Cryst. Liq. Cryst. Inc. Nonlinear Opt.* **2006**, *154*, 289.
- [17] P. S. Drzaic, *Liq. Cryst.* **2007**, *3*, 1543.
- [18] O. Levy, *Phys. Rev. Lett.* **2001**, *86*, 2822.

- [19] A. Fernández-Nieves, D. R. Link, D. Rudhardt, D. A. Weitz, *Phys. Rev. Lett.* **2004**, 92, 105503.
- [20] M. S. Kim, F. Serra, *RSC Adv.* **2018**, 8, 35640.
- [21] J. J. S. O'Neill, P. S. Salter, M. J. Booth, S. J. Elston, S. M. Morris, *Nat. Commun.* **2020**, 11, 2203.
- [22] M. S. Kim, F. Serra, *Adv. Opt. Mater.* **2020**, 8, 1900991.
- [23] B. Kim, B. K. Kim, D.-J. Lee, G.-Y. Shim, H.-R. Kim, H. G. Kim, J.-H. Baek, J.-S. Park, J.-H. Lee, K.-I. Joo, Y. Choi, *Appl. Opt.* **2018**, 57, 119.
- [24] Y.-C. Shin, J.-S. Park, K.-I. Joo, H. G. Kim, R. Manda, J.-C. Choi, H.-R. Kim, Y.-C. Shin, R. Manda, J.-C. Choi, H.-R. Kim, J.-S. Park, H. G. Kim, K.-I. Joo, *Adv. Mater. Interfaces* **2022**, 9, 2101919.
- [25] S. C. Jain, D. K. Rout, *J. Appl. Phys.* **1998**, 70, 6988.
- [26] M. S. Kim, M. Kim, J. H. Jung, K. S. Ha, S. Yoon, E. G. Song, A. K. Srivastava, S.-W. Choi, G.-D. Lee, S. H. Lee, *Dig. Tech. Pap. - Soc. Inf. Disp. Int. Symp.* **2009**, 40, 1615.
- [27] M. S. Kim, Y. J. Lim, S. Yoon, S.-W. Kang, S. H. Lee, M. Kim, S.-T. Wu, *J. Phys. D.: Appl. Phys.* **2010**, 43, 145502.
- [28] M. S. Kim, Y. J. Lim, S. Yoon, M.-K. Kim, P. Kumar, S.-W. Kang, W.-S. Kang, G.-D. Lee, S. H. Lee, *Liq. Cryst.* **2011**, 38, 371.
- [29] M. S. Kim, L. C. Chien, *Soft Matter* **2015**, 11, 8013.
- [30] M. S. Kim, R. K. Mishra, R. Manda, G. Murali, T.-H. Kim, M.-H. Lee, M. Yun, S. Kundu, B.-S. Kim, S. H. Lee, *RSC Adv.* **2017**, 7, 16650.
- [31] R. Manda, S. Pagidi, Y. J. Heo, Y. J. Lim, M. S. Kim, S. H. Lee, *Adv. Mater. Interfaces* **2020**, 7, 1901923.
- [32] R. Manda, S. Pagidi, Y. Heo, Y. J. Lim, M. S. Kim, S. H. Lee, *NPG Asia Mater* **2020**, 12, 42.
- [33] I. Amimori, J. N. Eakin, J. Qi, G. Skačej, S. Žumer, G. P. Crawford, *Phys. Rev. E* **2005**, 71, 031702.
- [34] S. J. Kłosowicz, M. Aleksander, P. Obrzut, *Proc. SPIE* **2005**, 59470M, 5947.
- [35] P. Oswald, A. Dequidt, A. Zywockiński, *Phys. Rev. E* **2008**, 77, 061703.
- [36] M. Sadati, J. A. Martinez-Gonzalez, Y. Zhou, N. T. Qazvini, K. Kurtenbach, X. Li, E. Bukusoglu, R. Zhang, N. L. Abbott, J. P. Hernandez-Ortiz, J. J. DePablo, *Sci. Adv.* **2020**, 6, eaba6728.
- [37] N. Iwata, K. Yazawa, M. Tokita, *Liq. Cryst.* **2019**, 46, 1881.
- [38] Y. Kinose, K. Sakakibara, O. Sato, Y. Tsujii, *ACS Appl. Polym. Mater.* **2021**, 3, 2618.
- [39] S. Pagidi, H. S. Park, D. Y. Lee, M. S. Kim, S. H. Lee, *J. Mol. Liq.* **2022**, 350, 118540.
- [40] K. Rijeesh, H. Higuchi, Y. Okumura, J. Yamamoto, H. Kikuchi, *Polymer* **2017**, 116, 447.
- [41] D. Yoshizawa, Y. Okumura, J. Yamamoto, H. Kikuchi, *Polym. J.* **2019**, 51, 667.
- [42] Y. Cui, R. S. Zola, Y. C. Yang, D. K. Yang, *J. Appl. Phys.* **2012**, 111, 063520.
- [43] V. P. Vorflusev, H. S. Kitzerow, V. G. Chigrinov, *Appl. Phys. Lett.* **1998**, 70, 3359.
- [44] C. J. Cheng, L. Y. Chu, R. Xie, X. W. Wang, *Chem. Eng. Technol.* **2008**, 31, 377.
- [45] M. Yasuno, M. Nakajima, S. Iwamoto, T. Maruyama, S. Sugiura, I. Kobayashi, A. Shono, K. Satoh, *J. Membr. Sci.* **2002**, 210, 29.